

# Validation of a simplified micromodel for analysis of infilled RC frames exposed to cyclic lateral loads

Davorin Penava<sup>1</sup> · Vladimir Sigmund<sup>1</sup> · Ivica Kožar<sup>2</sup>

Received: 30 May 2015 / Accepted: 3 May 2016 / Published online: 7 May 2016  
© Springer Science+Business Media Dordrecht 2016

**Abstract** An RC frame structure with masonry infill walls (“framed-masonry”) exposed to lateral loads acts as a composite structure. Numerical simulation of framed-masonry is difficult and generally unreliable due to many difficulties and uncertainties in its modelling. In this paper, we reviewed the usability of an advanced non-linear FEM computer program to accurately predict the behaviour of framed-masonry elements when exposed to cyclic lateral loading. Numerical results are validated against the test results of framed-masonry specimens, with and without openings. Initial simplified micromodels were calibrated by adjustment of the input parameters within the physically justifiable borders, in order to obtain the best correlation between the experimental and numerical results. It has been shown that the use of simplified micromodels for the investigation of composite masonry-infilled RC frames requires in-depth knowledge and engineering judgement in order to be used with confidence. Modelling problems were identified and explained in detail, which in turn offer an insight to practising engineers on how to deal with them.

**Keywords** Infilled frame · Framed-masonry · Simplified micromodel · Calibration · Validation

## 1 Introduction

After earthquakes, field investigations and research results have shown that masonry infill placed within a structural RC frame (“framed-masonry”) has both positive and negative effects (Negro and Colombo 1997) (Hashemi and Mosalam 2006) on the seismic

---

✉ Davorin Penava  
davorin.penava@gfos.hr

<sup>1</sup> Faculty of Civil Engineering Osijek, Josip Juraj Strossmayer University of Osijek, Osijek, Croatia

<sup>2</sup> Faculty of Civil Engineering, University of Rijeka, Rijeka, Croatia

performance of the system. The new composite “framed-masonry” system has smaller drifts and deformations in structural members, together with shear resistance of higher storey and global energy dissipation. On the other hand, the infill wall presence can have an extremely negative effect on the surrounding frame in terms of shear failure of captive columns, depending on the wall strength, as given in, e.g., FEMA 306 (ATC 1998). Infill walls, comprising masonry units with high horizontal strength, e.g., solid clay bricks of Group 1 as in EN 1996-1-1 (CEN 2005), can cause such an effect. Hollow clay masonry units, e.g., Group 2 in EN 1996-1-1 (CEN 2005), with weak horizontal strength do not cause captive column effects and enable plastic hinge formation at the column-ends (Sigmund and Penava 2014). The increase of shear forces and reduction of drift capacity lead to serious vulnerabilities, unless proper proportioning is exercised. Therefore, EN 1998-1 (CEN 2004a) does not encourage designers to profit from the beneficial effects of masonry infill in relation to the seismic response of RC frame structures; rather, it warns them against the adverse effects.

Special problems are presented by framed-masonry structural elements in the presence of the opening in the masonry infill. Tested within the experimental campaign (Penava 2012) were 10 framed-masonry specimens with one storey and one bay, as well as an opening in the masonry infill wall, under quasi-static cyclic loading. Midsize window and door openings were located centrally and eccentrically. Although not accounted for in the design, the tests revealed that the presence of masonry infill with openings improved system behaviour at drift levels of up to 1 %. During the test, openings did not influence the initial stiffness and strength at low drift levels. Their presence became noticeable at higher drift levels, where they lowered the energy dissipation capacity of the system. The infill wall had a multiple failure mechanism, which depended on the opening’s height and position. No negative effects of the infill on the frame were observed. The infill’s contribution could be deemed positive as it enhanced the overall structural performance level.

For frames with competent walls, the challenge for safe and economical design is to be able to take advantage of the stiffening, while making certain that the increase in shear forces and reduction in drift capacity do not handicap performance. Therefore, proper numerical modelling of framed-masonry structures is required. There are many distinct approaches for their modelling, which could be divided into macromodels (no separate masonry units in the model), simplified micromodels (separate masonry units with interface elements) and micromodels (separate masonry units and mortar in the model) (Asteris et al. 2011a, 2013). The use of mathematical macromodels fails to capture the interaction between the bounding frame and the infill wall. On the other hand, parameter uncertainties involved in the mathematical micro modelling of framed-masonry elements, which combine two brittle materials, make their use unreliable. In the case of a competent wall with an opening, among anticipated failure modes (Asteris et al. 2011b) there is the bed joint sliding failure that tends to occur in weakened planes above and below the opening. The infill decomposes itself into subcomponents (Sigmund and Penava 2014) and the infill bearing capacity is determined by the capacity of the critical subcomponent. The macromodels, which are not capable of describing the bed joint sliding of the infilled frame system, cannot represent the influence of the infill on the surrounding frame (Crisafulli et al. 2000). If the masonry infill is modelled as described by (Dawe et al. 2001; Ghosh and Amde 2002; Meharbi and Shing 2003; Ellul and D’Ayala 2012) the frame - infill interaction is observed more accurately while still allowing global structural analysis. However, usage of global masonry properties, instead of its constituents as in micromodels, makes the structural response prediction more uncertain, especially under different loading

scenarios. Micromodels are not practical for global analysis but if properly used, they can replace experiments. Independent of the modelling approach calibration is always required.

The current paper is focused on the presentation of problems encountered when trying to develop an adequate, simplified non-linear micromodel element model. That model is an irreplaceable tool for the estimation of shear resistance capacity of framed-masonry, with or without openings. In order to test the ability of the available simplified micromodel to predict the behaviour of infilled frames accurately, we validated numerical results against the experimental ones for framed-masonry specimens with openings of various sizes and positions. The correlation between the calculated and experimentally obtained results has been validated on the basis of the observed failure mechanisms as well as elements of the resistance envelope curve needed for the design and evaluation of “framed-masonry” structures. Validation deals with the model’s ability to represent the real process according to its intended purpose. In our case, it is the ability of a computer program to predict the failure of a confined masonry wall. Here, we distinguish statistically-based validation, which is grounded on a large number of experiments, and a conceptual validation, predicated on a large-scale experiment. The latter case is common in civil engineering when we perform expensive experiments, usually on only one large structure. The obtained data are not statistically significant, but serve as a proof of concept. It is in accordance with the fact that the validation procedure does not imply that the experimental data are always correct (Oberkampff and Roy 2010).

It has been shown that the use of a simplified micromodel for the investigation of composite framed-masonry structures requires an in-depth knowledge of the applied numerical model and sound engineering judgement. Modelling problems were identified in the modelling of RC frame elements and masonry infill walls. Identified problems are explained in detail and could give an insight to practising engineers on how to deal with them. Calibrated models were able to completely capture the failure mechanisms, while the accuracy errors in predicting the elements of the resistance envelope curves were kept within the acceptable limits, thereby making it adequate for further investigation.

## 2 Materials and methods

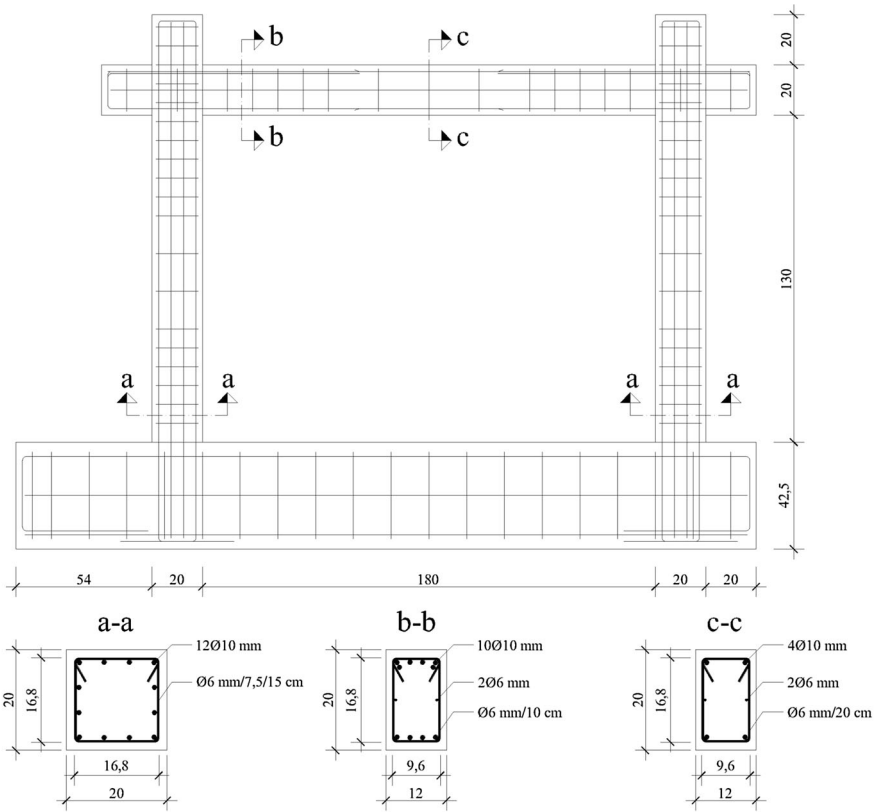
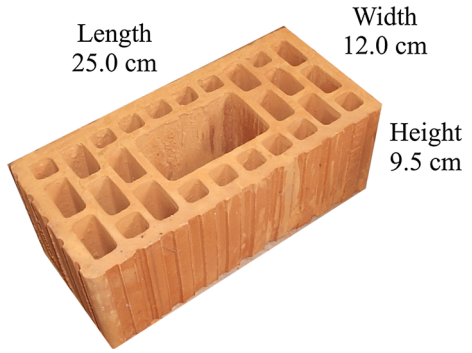
### 2.1 Description of the specimen tests

In (Penava 2012), 10 framed-masonry specimens were tested at a scale of 1:2.5. Frames were designed as medium-ductility frames (DCM) in compliance with EN 1992-1-1 (CEN 2004b) and EN 1998-1 (CEN 2004a). Masonry infill was made using hollow clay masonry units (Fig. 1), which belong to Group 2, and mortar joints of M5 class mortar (EN 1996-1-1 (CEN 2005)). Specimens (Fig. 2) were tested under quasi-static cyclic lateral loading applied at the beam-ends and under a near constant vertical load of 365 kN applied at the column-ends.

Static pushover loading was applied after large cracks in the infill occurred (DG 3-EMS 98 (Grünthal et al. 1998)); this is shown as a dashed line in Fig. 6. A detailed description of the test rig, the structural material properties and the loading scheme can be found in (Sigmund and Penava 2014).

Test specimens were divided into three groups. The first group consisted of four specimens with an unconfined opening, i.e., a door or window, centrically or eccentrically positioned. The second group had vertical tie column elements around the opening. The

**Fig. 1** Hollow clay masonry units used




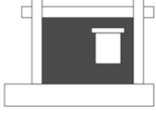
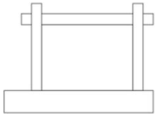
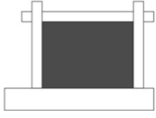


**Fig. 2** Infilled frames tested by (Penava 2012)

third group had two reference specimens, i.e., framed- masonry without an opening and a bare reinforced concrete frame. The opening area was selected around  $A_o \approx 2.0 \text{ m}^2$  as the mean of the two criteria for execution of the confining elements around them, i.e.,  $A_o > 1.5 \text{ m}^2$  (EN 1998-1 (CEN 2004a)) and  $A_o > 2.5 \text{ m}^2$  (Tomažević 1999), and in compliance with standard opening measures (Neufert and Neufert 2012). Specimens of groups I and III are shown in Table 1, where  $A_o = h_o * l_o$  is the area of an opening,  $A_i = h_i * l_i$  is the area of masonry infill wall,  $l_o$  is the opening length,  $h_o$  is the opening height,  $h_i = 1.3 \text{ m}$  is the infill wall height,  $l_i = 1.8 \text{ m}$  is the infill wall length,  $e_o$  is the opening eccentricity,  $t_i = 0.12 \text{ m}$  is the infill wall thickness and  $P$  is the parapet wall height.

Test results are presented according to the resistance envelope curves (peaks of the second cycles), values of the secant stiffness at characteristic drifts and observed failure mechanisms. Characteristic damage grades of the framed-masonry specimens were

**Table 1** Classification and description of the specimens

Specimen		Appearance of the specimen	Opening		Description
Group	Mark		Type and area	Position	
I	1		Door $l_o/h_o = 0.35/0.90 \text{ m}$ $A_o = 0.32 \text{ m}^2$ $A_o/A_i = 0.14$	Centric $e_o = l_i/2 = 0.90 \text{ m}$	Specimens without confinement
	2		Window $l_o/h_o = 50.0/60.0 \text{ cm}$ $A_o = 0.30 \text{ m}^2$ $A_o/A_i = 0.13$	Centric $e_o = l_i/2 = 0.90 \text{ m}$ $P = 0.40 \text{ m}$	
	3		Door $l_o/h_o = 0.35/0.90 \text{ m}$ $A_o = 0.32 \text{ m}^2$ $A_o/A_i = 0.14$	Eccentric $e_o = h_i/5 + l_o/2 = 0.44 \text{ m}$	
	4		Window $l_o/h_o = 50.0/60.0 \text{ cm}$ $A_o = 0.30 \text{ m}^2$ $A_o/A_i = 0.13$	Eccentric $e_o = h_i/5 + l_o/2 = 0.44 \text{ m}$ $P = 0.40 \text{ m}$	
II	1		–	–	Reference specimens
	2		–	–	

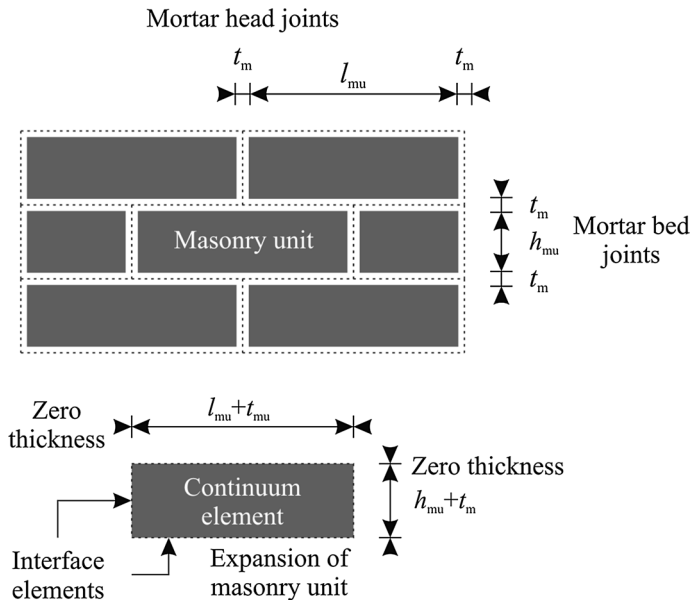
observed as being 0.1 % for slight (DG1), 0.2–0.3 for moderate (DG 2), 0.5 for heavy (DG 3) and 1.0 % for precollapse (DG 4). These damage grades are in compliance with the EMS-98 damage scale (Grünthal et al. 1998) and occur within the masonry infill. Also observed was the sequenced failure mechanism of the masonry infill wall in the case of an opening without confinement. It first occurred as the bed joint sliding failure above the opening due to weakened horizontal planes (caused by the presence of an opening) and continued as the diagonal tensile or the bed joint sliding failure of the formed masonry pier (a crucial part of the masonry infill wall for seismic resistance). The formed masonry pier, located in the wall with an unconfined opening, has been predetermined by the opening's height and bed joint sliding in the weakened planes.

By comparing the measured resistance envelope curves between the framed-masonry and the bare frame, significant increases in secant stiffness and a load carrying capacity of up to three times have been observed. Similar resistance envelope curves were obtained for all framed-masonry specimens, regardless of the opening.

Tested specimens with confinements around the opening are not considered in this paper.

## 2.2 Description of the simplified micromodel

To describe the non-linear behaviour of concrete, masonry and steel, as well as their interactions, a computer program was run, which used incorporated libraries, including a large number of finite elements, robust solution strategies and a variety of material models. As their level of sophistication increased, using such a program for the investigation of composite structures with complex interfacial boundary conditions has become common. We checked its usability for an engineering analysis of the framed-masonry composite structures on the tested specimens. Since only in-plane loading was present, a two-dimensional (2D) simplified micromodel was selected for the masonry infill wall (Fig. 3).



**Fig. 3** Simplified micromodel used

Masonry units and the mortar-masonry interface were considered separately and, in this way, it was possible to capture the sequenced failure of the masonry infill wall and to avoid modelling of the mortar. For each material, the most appropriate constitutive law capable of describing its structural behaviour was used. Initial input data for each material model were tested on material properties obtained by standard material tests, as required by European structural standards. Mean values of the tested properties of all specimens were used. Additional data for each material model were obtained from (Bažant and Oh 1983a, b; Saneinejad 1990a, b; Bažant and Planas 1997; Cervenka et al. 2012).

The smeared crack approach has been adopted for crack modelling.

### 2.2.1 Reinforced concrete material model

The fracture-plastic constitutive law, known as the NonLinCementitious2 material model, was adopted for the reinforced concrete frame and the lintel. It has the ability to describe the fat unloading curve, while its inability to describe the shear cracking, due to the smeared crack approach, is not emphasized, since failures of this type did not occur in the tests. The rotated crack model was found to be more suitable for cyclic analysis than the fixed crack model (see (Cervenka Consulting 2012) for the theoretical background). The fixed crack model was discarded because it caused early calculation instabilities. The input data used for the concrete model are given in Table 2 (parameters marked with an \* were added after they were found to be necessary for calibration).

Longitudinal and transversal steel reinforcements were modelled as truss elements. For the cyclic material model, the Menegotto-Pinto model (Cervenka et al. 2012) was defined with a bilinear primary curve with strain hardening. In order to resemble the physical model, a smeared modelling approach for the transversal reinforcement was not used.

**Table 2** Initial concrete properties for material model NonLinCementitious2

Description	Symbol	Value	Units
Elastic modulus	$E$	41,000	MPa
Poisson's ratio	$\mu$	0.2	–
Tensile strength	$f_t$	4	MPa
Compressive strength	$f_c$	–58	MPa
Specific fracture energy	$G_f$	$1.20 \times 10^{-4}$	MN/m
Critical compressive displacement	$w_d$	$-1.0 \times 10^{-3}$	m
Eccentricity, defining the shape of the failure surface	Exc	0.52	–
Multiplier for the direction of the plastic flow	$\beta$	0	–
Crack model coefficient (1.0 for Fixed, 0.0 for Rotated)	–	0	–
Plastic strain at compressive strength	$\epsilon_{CP}$	$-1.417 \times 10^{-3}$	–
Reduction of comp. strength due to cracks	$f_{c,LIM}$	0.1	–
Crack shear stiff. factor	$s_F$	20	–
Aggregate size	–	0.016	m
Crack spacing*	$s_{max}$	0.125	m
Tension stiffening*	$c_{ts}$	0.4	–

**Table 3** Initial reinforcement properties for cycling reinforcement

Description	Symbol	Value	Units
Elastic modulus	$E$	210,000	MPa
Yield strength	$\sigma_y$	550	MPa
Ultimate strength	$\sigma_t$	650	MPa
Strain at ultimate strength	$\varepsilon_{im}$	0.01	–
Bauschinger effect exponent	$R$	20	–
Menegotto–Pinto model parameter	$C1$	0.925	–
Menegotto–Pinto model parameter	$C2$	0.15	–

Bond-slip of the reinforcement was neglected, but the contribution of the reinforcement in compression was included. Input data of the reinforcement are presented in Table 3.

### 2.2.2 Masonry-infilled material models

The SBeta material model was selected (with the rotated crack model) for the hollow clay masonry units, as it has the ability to represent the units' quasi-brittle nature. The properties of masonry units, which are parallel to the head joints (the direction of the hollows), required by the material model type SBeta are given in Table 4, while the properties parallel to the bed joints (perpendicular to the hollows) are given in Table 5. They were required because of the masonry units' orthotropic characteristics; the procedure for obtaining them is described later in the text.

The contact between the masonry units, as well as between the masonry units and the frame (the mortar in the physical model), was described by the interface material model. The model is based on the Mohr–Coulomb criterion with tension cut-off and requires  $K_{nn}$  and  $K_{tt}$ , which respectively represent the initial elastic normal and shear stiffness. They are purely numerical values and difficult to estimate accurately in light of the zero thickness of the interface (in the simplified micromodel). They were calculated using the expressions from (Cervenka et al. 2012) as  $K_{nn} = E/t$  and  $K_{tt} = G/t$ , where  $E$  and  $G$  are respectively the modulus of elasticity and the shear of the surrounding material, and  $t$  is the thickness of the mortar joint. An expression from (Lourenço et al. 1995) for estimating stiffness, which combines the modulus of elasticity of mortar and masonry units, was found to be inadequate in our case. Our hollow clay masonry units were orthotropic, with the modulus of elasticity in the horizontal direction lower than that in the mortar, in turn producing negative stiffness values for the head joints. The properties of bed and head joints are given separately in Tables 6 and 7, respectively.

Material properties for the lintel were assigned by default values, based on the concrete compressive strength of 30 MPa, which were obtained by conducting tests in compliance with EN 12390-3 (CEN 2009). The other parameters were adopted as for the frame material model. These data remained unchanged due to the minor role of the lintel in the calculations. To keep the model simple, contact between the beam and the infill and the column and the infill and contact between masonry units were the same. In the physical model, the contact with the beam was filled sideways with mortar, and the axial load present on the columns during the experiment, made the contact more efficiently.



**Table 4** Initial properties of the hollow clay masonry units parallel to the head joints

Description	Symbol	Value	Units
Elastic modulus	$E$	5650	MPa
Poisson's ratio	$\mu$	0.1	–
Tensile strength	$f_t$	1.8	MPa
Compressive strength	$f_c$	–17.5	MPa
Type of tension softening	Exponential		
Specific fracture energy	$G_f$	$0.45 \times 10^{-4}$	MN/m
Crack model	Rotated		
Compressive strain at compressive strength in the uniaxial compressive test	$\varepsilon_c$	$-1.358 \times 10^{-3}$	–
Reduction of compressive strength due to cracks	–	0.8	–
Type of compression softening	Crush Band		
Critical compressive displacement	$w_d$	$-5.0 \times 10^{-4}$	m
Shear retention factor	Variable		
Tension–compression interaction	Linear		

**Table 5** Initial properties of the hollow clay masonry units parallel to bed joints

Description	Symbol	Value	Units
Elastic modulus	$E$	850	MPa
Poisson's ratio	$\mu$	0.1	–
Compressive strength	$f_c$	–2.8	MPa

**Table 6** Initial properties of bed joints

Description	Symbol	Value	Units
Normal stiffness	$K_{nn}$	$5.65 \times 10^5$	MN/m <sup>3</sup>
Tangential stiffness	$K_{tt}$	$2.57 \times 10^5$	MN/m <sup>3</sup>
Cohesion (variance 28 %)	$c$	0.35	MPa
Tensile strength (variance 20 %)	$f_t$	0.2	MPa
Friction coefficient (variance 28 %)	–	0.24	–
Minimum normal stiffness	$K_{nn,min}$	$5.65 \times 10^2$	MN/m <sup>3</sup>
Minimum tangential stiffness	$K_{tt,min}$	$2.57 \times 10^2$	MN/m <sup>3</sup>
Function tension softening–hardening	Not used		
Function cohesion softening–hardening	Used		

**Table 7** Initial properties of head joints

Description	Symbol	Value	Units
Normal stiffness	$K_{nn}$	$8.50 \times 10^4$	MN/m <sup>3</sup>
Tangential stiffness	$K_{tt}$	$3.86 \times 10^4$	MN/m <sup>3</sup>
Cohesion	Adopted from the bed joints		
Tensile strength			
Friction coefficient			
Minimum normal stiffness	$K_{nn,min}$	$8.50 \times 10^1$	MN/m <sup>3</sup>
Minimum tangential stiffness	$K_{tt,min}$	$3.86 \times 10^1$	MN/m <sup>3</sup>

### 2.2.3 Mesh properties and test simulation

The specimen model was assembled by using isoparametric plane finite elements (9-node quadrilateral and 6-node triangular) for concrete and masonry units, and truss elements (3-nodes) for reinforcement and gap elements with non-linear geometry for the interface. Mesh size was very important for quality of the numerical results. Finer mesh (i.e., with a mesh size = 1/10 of the structural element) led to much longer calculation time without significant improvements in accuracy. Coarser mesh (i.e., with a mesh size = 1/2 of the element) turned out incorrect results. A finite elements mesh, with an element length equal to one quarter of the structural element size, was assigned. In this way, the RC columns and beams were divided into at least four elements in a section. For the masonry units, coarser mesh could be used, but we used the same.

Displacement and force boundary conditions were selected to correspond with those from the tests (direct shear), including the use of a fixed-base beam and the prevention of vertical movement in the column-ends. Forces were applied at the beam-ends. The vertical load was applied in five steps until the targeted value was achieved. The horizontal load/displacements were then applied in increments of 10kN. In order to simulate the proper load distribution, steel pads (plane finite elements with a linear elastic constitutive law) were placed at the beam- and column-ends, as in the tests.

The Newton–Raphson method was used to solve the non-linear equations. It was selected before the arc-length method because of the rightful presentation of the specimen's load–displacement relationship during calculations (convergence of displacement only). The selected approach (force-controlled) in calculations is completely compatible with a two-way loading approach in tests (see Sect. 2.1). This is because the specimen, after reaching the highest load in calculations, yielded and produced an equivalent reaction to those in the tests. Additionally, modelling of the exact approach, as in the tests, would not be meaningful for possible extrapolations of the study, since it is difficult to predict yielding occurrence in the specimen in order to apply a pushover approach.

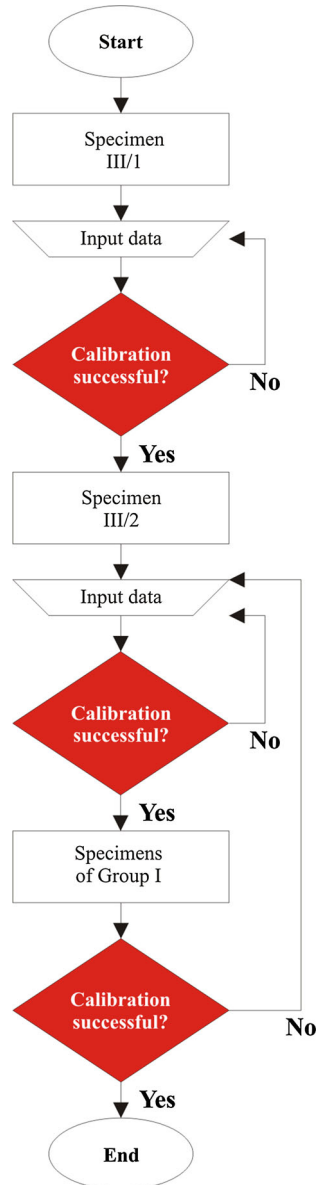
## 3 Analysis and results

The numerical model of framed-masonry specimens was set up according to the described procedure, while further modifications were undertaken in order to correlate the calculated results with the experimentally obtained ones. Obtained secant stiffness values and failure mechanisms were used for the evaluation.

The secant stiffness relates to two parameters simultaneously (base shear force  $F_b$  and the displacement  $d$ ). Three particular values of the secant stiffness were compared:

(a) differences in the secant stiffness at four damage levels were calculated and then normalized to the secant stiffness value at DG1; (b) differences were expressed as the mean value at four damage levels separately for positive and negative cycles and (c) differences were expressed as the joint mean value of both positive and negative loading cycles. Calibration was considered successful when the numerical and experimental results (differences) were within the range of acceptable tolerance (error < 15 %). The failure mechanism of the tested and calibrated numerical models ought to be identical, which is a factor considered to be the ultimate criterion of successful calibration.

**Fig. 4** Calibration flow chart



Calibration of the material and numerical models has been conducted in a sequenced manner, from the simple to the more complex, in order to reduce the number of parameters that have a high influence on the results. The first to be modelled was the bare frame specimen (Specimen III/1), then the framed-masonry specimen (Specimen III/2) and, finally, the framed-masonry specimens with openings. The presence of openings in infill panels constitutes an important uncertainty in the evaluation of behaviour, given the large number of variables and uncertainties involved. At each step, a parametric analysis was performed until the correlation between the measured and calculated behaviour was satisfactory, according to the previously set targets. A calibration flow chart is given in Fig. 4.

### 3.1 Calibration of the bare frame model

Calibration started with the initial material properties, as given in Sect. 2.2.1 (Tables 2, 3). Additional modifications were undertaken:

- The transverse reinforcement area was increased by an amount equal to the area of the corresponding longitudinal reinforcement, as suggested by (Pryl and Cervenka 2013). This should compensate the missing dowel effect in the reinforcement truss elements.
- The lowest transversal bar was moved upwards from the columns' toes, with its area multiplied 100 times in order to increase its stiffness. This was necessary for the prevention of excessive (unrealistic) deformation of the plastic hinge zone.
- Using the initial material properties and engineering corrections of the numerical model required correlation of the test and numerical results, which was not achieved. At higher load cycles, a plastic hinge zone at a column's toe experienced extensive cracking, which led to severe and sudden softening, as well as the model suddenly yielding. Besides these factors, there was no pronounced hysteresis loop area within corresponding loading cycles. This problem was solved by inclusion of the tension stiffening option, in compliance with (CEB 1993) and (Cervenka et al. 2012), and calculation of the crack spacing value (Bažant and Oh 1983a, b Bažant and Planas 1997), as given in Table 2. The latter was needed to prevent non-localization damage and justified by use of a high reinforcement ratio in this area. Introduction of these modifications ensured dominant bending behaviour of the frame structure.

Results are presented using hysteresis loops and response envelope (primary) curves in Fig. 6. Displacements ( $d$ ) and inter-storey drift ratios ( $IDR = d/h_i + h_b/2$  where  $h_b =$  - beam height) are presented on the horizontal axis, while base shear ( $F_b$ ) and normalized base shear ( $F_b/F_{b,max,f}$ , where  $F_{b,max,f}$  = base shear force of the bare frame) appear on the vertical axis. Secant stiffness values ( $K = F_b/d$ ) in characteristic inter-storey drift ratios (damage grades) are given in Tables 8, 9 and 10, where indices  $t$  and  $c$  designate test and calculated values, respectively.

Observed failure mechanisms are given for the pushover direction (see Sect. 2.1: Description of the specimen tests). The calculated and experimental results are given in Fig. 6.

### 3.2 Calibration of the framed-masonry models

#### 3.2.1 Problems encountered during modelling of the hollow clay masonry units

When we tried to simulate the results of the Specimen III/2 model, there was a problem with the modelling of the orthotropic hollow clay masonry units. The material model only

**Table 8** Correlation between test and calculations in terms of secant stiffness at four damage levels

Spec.	IDR (%)	Positive cycles					Negative cycles					Total mean (%)	
		$K_t$ (kNmm)	$K_c$ (kNmm)	$m = K_t/K_{t,0}$ (-)	$n = K_c/K_{c,0.1}$ (-)	$m-n$ (%)	Mean (%)	$K_t$ (kNmm)	$K_c$ (kNmm)	$m = K_t/K_{t,0}$ (-)	$n = K_c/K_{c,0.1}$ (-)		$m-n$ (%)
III/1	0.1	45	42	1.00	0.93	6.7	-1.7	-60	-42	1.00	0.70	30.0	7.1
	0.2	34	37	0.76	0.82	-6.7		-48	-38	0.80	0.63	16.7	
	0.5	22	23	0.49	0.51	-2.2		-22	-28	0.37	0.47	-10.0	
	1.0	12	14	0.27	0.31	-4.4		-16	-21	0.27	0.35	-8.3	

**Table 9** Correlation between tested and calculated secant stiffness at four damage levels (first approach)

Spec.	IDR (%)	Positive cycles					Negative cycles					Total mean (%)	
		$K_t$ (kNmm)	$K_c$ (kNmm)	$m = K_t/K_{t,0}$ (-)	$n = K_c/K_{c,0.1}$ (-)	$m-n$ (%)	Mean (%)	$K_t$ (kNmm)	$K_c$ (kNmm)	$m = K_t/K_{t,0}$ (-)	$n = K_c/K_{c,0.1}$ (-)		$m-n$ (%)
III/2	0.1	142	53	1.00	0.37	62.7	29.2	-150	-53	1.00	0.35	64.7	27.8
	0.2	93	40	0.65	0.28	37.3		-96	-40	0.64	0.27	37.3	
	0.5	40	23	0.28	0.16	12.0		-47	-20	0.31	0.13	18.0	
	1.0	19	12	0.13	0.08	4.9		-	-13	0.00	0.09	-8.7	
													28.5

**Table 10** Correlation between tested and calculated secant stiffness at four damage levels (second approach)

Spec.	IDR (%)	Positive cycles					Negative cycles					Total mean (%)	
		$K_1$ (kNmm)	$K_c$ (kNmm)	$m = K_1/K_{1,0.1}$ (-)	$n = K_c/K_{c,0.1}$ (-)	$m-n$ (%)	Mean (%)	$K_1$ (kNmm)	$K_c$ (kNmm)	$m = K_1/K_{1,0.1}$ (-)	$n = K_c/K_{c,0.1}$ (-)		$m-n$ (%)
I/1	0.1	137	104	1.00	0.76	24.1	13.5	-145	-108	1.00	0.74	25.5	14.3
	0.2	95	53	0.69	0.39	30.7		-88	-59	0.61	0.41	20.0	
	0.5	33	23	0.24	0.17	7.3		-26	-26	0.18	0.18	0.0	
I/2	1.0	-	11	0.00	0.08	-8.0		-17	-	0.12	0.00	11.7	
	0.1	163	109	1.00	0.67	33.1	16.0	-150	-126	1.00	0.84	16.0	14.8
	0.2	103	60	0.63	0.37	26.4		-87	-79	0.58	0.53	5.3	
I/3	0.5	42	23	0.26	0.14	11.7		-35	-	0.23	0.00	23.3	
	1.0	-	12	0.00	0.07	-7.4		-22	-	0.15	0.00	14.7	
	0.1	160	164	1.00	1.03	-2.5	13.4	-131	-61	1.00	0.47	53.4	30.7
I/4	0.2	93	60	0.58	0.38	20.6		-100	-46	0.76	0.35	41.2	
	0.5	37	-	0.23	0.00	23.1		-40	-21	0.31	0.16	14.5	
	1.0	20	-	0.13	0.00	12.5		-18	-	0.14	0.00	13.7	
II/2	0.1	142	124	1.00	0.87	12.7	9.9	-150	-51	1.00	0.34	66.0	25.7
	0.2	93	72	0.65	0.51	14.8		-96	-51	0.64	0.34	30.0	
	0.5	40	25	0.28	0.18	10.6		-47	-25	0.31	0.17	14.7	
III/2	1.0	19	17	0.13	0.12	1.4		-	-12	0.00	0.08	-8.0	
	0.1	142	147	1.00	1.04	-3.5	-0.4	-150	-151	1.00	1.01	-0.7	9.7
	0.2	93	83	0.65	0.58	7.0		-96	-84	0.64	0.56	8.0	
III/2	0.5	40	54	0.28	0.38	-9.9		-47	-	0.31	0.00	31.3	
	1.0	19	12	0.13	0.08	4.9		-	-	0.00	0.00	0.0	

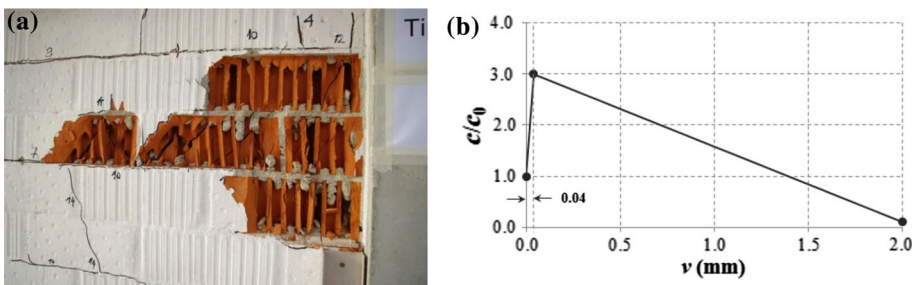
allowed for homogeneous (solid) material, while the physically orthotropic masonry units became solid bricks in the numerical model. After several trials, it was obvious that horizontal properties provided inadequate results, such that vertical properties were chosen as the representative ones. They are usually provided by the brick industry as being representative and are consequently easy to obtain. On the other hand, their disadvantage is mostly concerned with the behaviour of the infill wall when specimens are horizontally loaded, as observed in the tests. Solid masonry units are pushed rather than crushed, whereas hollow clay masonry units behave in the opposite manner. Crushing in the latter occurs due to their low horizontal strength and their reduced robustness. This so-called pillow effect could not be reproduced, which led to higher stresses on bed joints that were especially important in weakened horizontal planes due to the presence of openings. The thickness of the masonry units was kept constant, since the material properties were expressed by their gross values.

The orthotropic properties were modelled by different characteristics of head and bed joints. Mortar joint thickness was the same in both cases (10 mm) and has been modelled using the applied simplified micromodel by the interface element. Stiffness of the interface element was estimated on the basis of the stiffness of surrounding elements. Both normal and tangential stiffness of the head joints was calculated based on the modulus of elasticity and the shear in the horizontal direction (parallel to the bed joints) of the lower strength, respectively. The shear modulus was estimated based on the elastic relation among the  $E$ ,  $G$  and  $\mu$ . For the bed joints, properties in a vertical direction (parallel to the head joints) were used. At the contact with the surrounding frame, stiffness of the interface element was kept as it was between masonry units. This approach enabled successful correlation between the measured and calculated results, especially the failure mechanism. Use of different stiffness values affected stress paths (observed through cracks).

### 3.2.2 Problems encountered during modelling the interface elements

In the simplified micromodel, mortar joints were modelled as interface elements with zero thickness. They were crucial for the modelling of the masonry infill behaviour. For interface elements, a unique physical representation was implemented for bed joints as a consequence of mortar interlocking within the units' hollows (Fig. 5a). Three approaches were tried for bed joints, while the same characteristics of head joints remained in all cases.

In the first approach, contact properties of the interface elements—initial shear strength (cohesion), coefficient of internal friction and tensile strength (adhesion)—were obtained from tests conducted in compliance with EN 1052-3 (CEN 2007) and (Jäger 2012),



**Fig. 5** **a** Mortar interlocking with the units (*left*) and **b** cohesion hardening–softening function (*right*)



respectively. Those properties were used for bed and head joints. We found that the experimental and calculated results did not correlate with the values shown in Table 9.

For the second approach, the input data obtained from tests were replaced by recommended values from the literature (Saneinejad 1990a, b), which were approximately two times higher than the measured material data. Their purpose was to compensate for the weaknesses of the material model, although they were not physically justified. Experimental and calculated results correlated well for Specimen III/2, but not for the specimens of the Group I models. This could be attributed to the early bed joint sliding failure, due to the opening's presence (sliding along the bed joints was allowed, while the opening's side slid away) and because the masonry units were modelled as solid blocks (neglecting the mortar interlocking with the hollow clay masonry units). Results are given in Table 10.

The third approach proved to be the best correlation for framed-masonry specimens, both with and without openings. It consisted of the measured material data, as in the first approach, with the addition of a cohesion hardening–softening function as presented in Fig. 5b. Horizontal (shear) displacement ( $v$  in mm) is given on the horizontal axis, while the ratio of the cohesion to the initial cohesion ( $c/c_0$ ) is given on the vertical axis.

Cohesive models have a long tradition in the modelling of quasi-brittle materials (concrete, brick etc.), e.g., (Hillerborg et al. 1976). Finite element implementation employs cohesion (or an R-curve) to describe surface separation during the crack formation.

As mentioned in (Hillerborg et al. 1976), cohesion curve (or R-curve) parameters are very sensitive to the input conditions, such as the degree of triaxiality of the stress state along the crack, among others. The proposed approach assumes they are constant along the crack front. Consequently, they have to be determined for the structure under consideration (i.e., not from data in references, unless they deal with the exact same problem) by using some of the recommended procedures: the direct method or numerical optimization (including “trial and error”, “error minimization” or “neural network”). Cohesion curve parameters’ “cohesive strength”, “critical separation” and “cohesive energy” are connected by the curve shape, with usually only two of them having to be determined: either cohesive strength and energy or cohesive strength and separation (as in this paper).

Three characteristic points of the cohesion-softening function, as given in Fig. 5b, were established as follows:

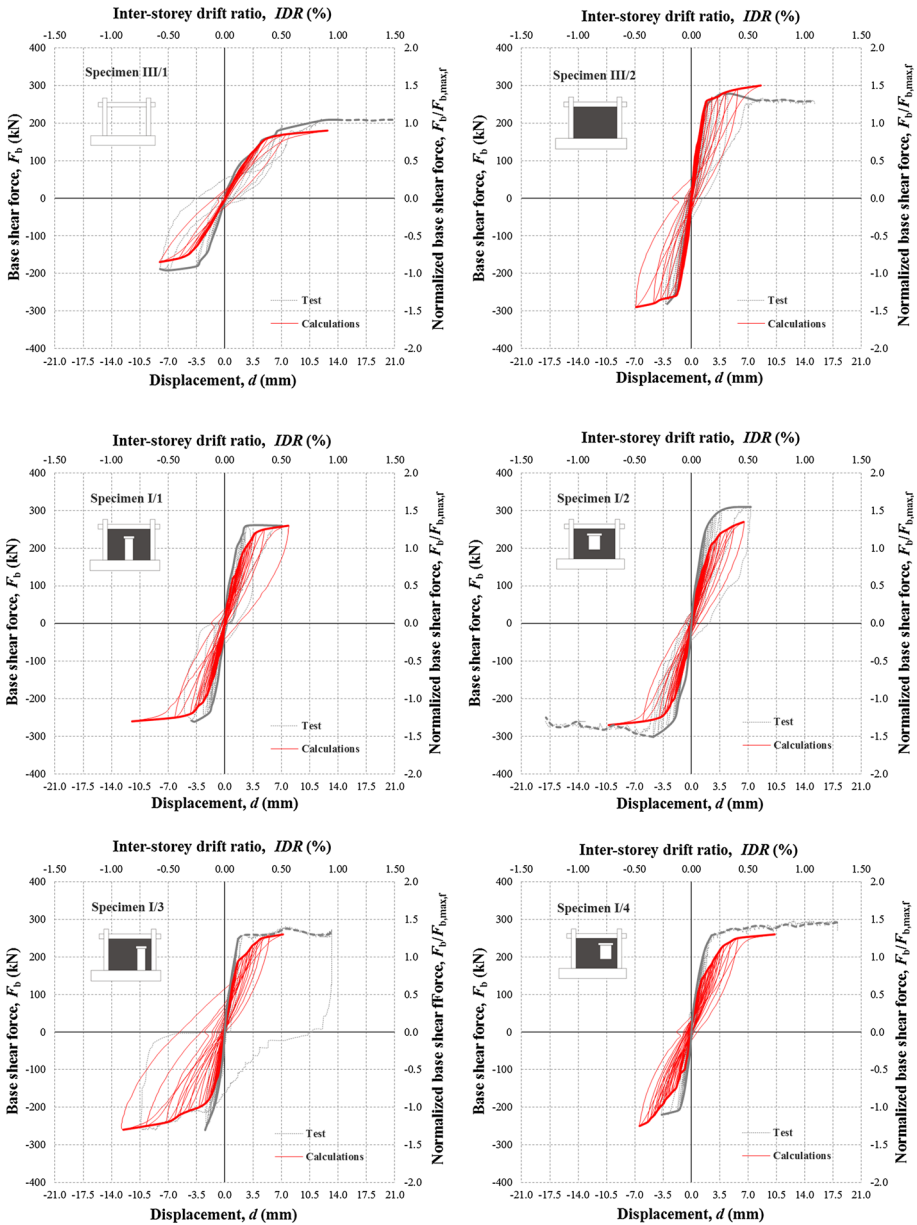
1.  $c = c_0$  for  $v = 0$  mm
2.  $c = 0.065 \cdot f_{mu}$  for  $v = 0.04$  mm based on expression

$$v = \gamma_{mu} \cdot h_{mu} = \frac{f_{mut}}{G_{mu}} \cdot h_{mu} = \frac{0.065 \cdot f_{mu}}{\frac{E_{mu}}{2 \cdot (1 + \mu_{mu})}} \cdot h_{mu} = \frac{0.065 \cdot 17.5}{\frac{5650}{2 \cdot (1 + 0.1)}} \cdot 95 = 0.04 \text{ mm}$$

where  $\gamma_{mu}$  is the shear deformation,  $f_{mut}$  and  $f_{mu}$  are the shear/tensile and compressive strength,  $E_{mu}$  is the modulus of elasticity,  $G_{mu}$  is the modulus of shear,  $h_{mu}$  is the height and  $\mu_{mu}$  is Poisson's ratio of the masonry unit (index mu), respectively.

3.  $c = 0$  for  $v = 2.0$  mm

The cohesion hardening–softening function was applied to the bed joints where mortar interlocks within the clay masonry unit's holes. This led to tensile (shear) failure of masonry units before and after contact. This has been recognized by the EN 1996-1-1 (CEN 2005) as the limit shear strength. In order to implement the function in the model, a post-initial shear strength function has been created. It has three characteristic points and two parts, i.e., a hardening part (between points 1 and 2) and a softening part (between points 2 and 3). The first point has the coordinate (0.1); the second is at the limit shear

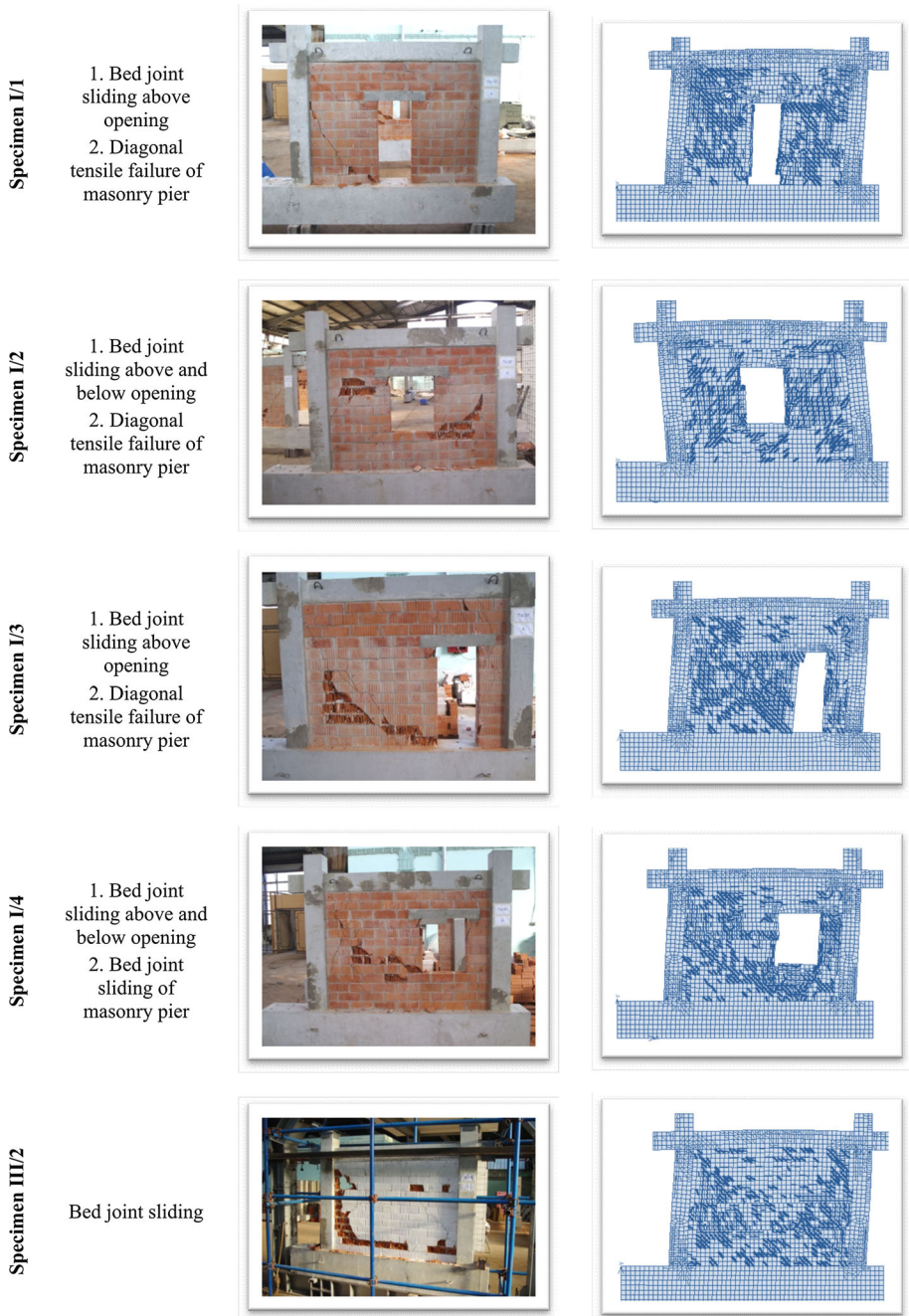


**Fig. 6** Experimental and calculated hysteresis loops and resistance envelope curves for all specimens with a cohesion-hardening function

strength (masonry unit tensile strength), along with the initial shear strength ratio and corresponding shear displacement (calculated from available material properties and unit geometry); and the third point is close to the zero coordinate in order to avoid numerical instability. This approach has been very sensitive to numerical instabilities (until the third

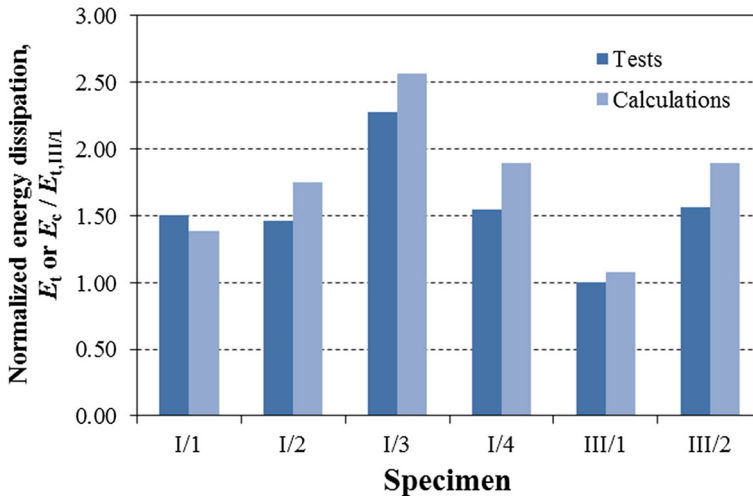
**Table 11** Correlation between tested and calculated secant stiffness at four damage levels (third approach)

Spec.	IDR (%)	Positive cycles					Negative cycles					Total mean (%)	
		$K_t$ (kNmm)	$K_c$ (kNmm)	$m = K_t/K_{t,0.1}$ (-)	$n = K_c/K_{c,0.1}$ (-)	$m-n$ (%)	Mean (%)	$K_t$ (kNmm)	$K_c$ (kNmm)	$m = K_t/K_{t,0.1}$ (-)	$n = K_c/K_{c,0.1}$ (-)		$m-n$ (%)
I/1	0.1	137	95	1.00	0.69	30.7	10.4	-145	-105	1.00	0.72	27.6	5.7
	0.2	95	74	0.69	0.54	15.3		-88	-77	0.61	0.53	7.6	
	0.5	33	33	0.24	0.24	0.0		-26	-38	0.18	0.26	-8.3	
	1.0	-	6	0.00	0.04	-4.4		-17	-23	0.12	0.16	-4.1	
I/2	0.1	163	100	1.00	0.61	38.7	11.8	-150	-107	1.00	0.71	28.7	10.8
	0.2	103	75	0.63	0.46	17.2		-87	-78	0.58	0.52	6.0	
	0.5	42	37	0.26	0.23	3.1		-35	-44	0.23	0.29	-6.0	
	1.0	-	19	0.00	0.12	-11.7		-22	-	0.15	0.00	14.7	
I/3	0.1	160	121	1.00	0.76	24.4	11.9	-131	-112	1.00	0.85	14.5	10.7
	0.2	93	77	0.58	0.48	10.0		-100	-63	0.76	0.48	28.2	
	0.5	37	36	0.23	0.23	0.6		-40	-34	0.31	0.26	4.6	
	1.0	20	-	0.13	0.00	12.5		-18	-24	0.14	0.18	-4.6	
I/4	0.1	142	95	1.00	0.67	33.1	10.9	-150	-83	1.00	0.55	44.7	13.7
	0.2	93	68	0.65	0.48	17.6		-96	-61	0.64	0.41	23.3	
	0.5	40	44	0.28	0.31	-2.8		-47	-39	0.31	0.26	5.3	
	1.0	19	25	0.13	0.18	-4.2		-	-28	0.00	0.19	-18.7	
III/2	0.1	151	162	1.00	1.07	-7.3	1.5	-151	-163	1.00	1.08	-7.9	-7.5
	0.2	94	83	0.62	0.55	7.3		-94	-104	0.62	0.69	-6.6	
	0.5	35	44	0.23	0.29	-6.0		-36	-42	0.24	0.28	-4.0	
	1.0	18	-	0.12	0.00	11.9		-17	-34	0.11	0.23	-11.3	



**Fig. 7** Calculated and actual failure mechanisms (*crack patterns*) of framed-masonry specimens

point has been adequately found) due to interaction between interface elements. This is due to the smeared crack approach used in the modelling of the masonry units. The properties of interface elements used for bed and head joints are given in Tables 6 and 7, respectively.



**Fig. 8** Normalized energy dissipation with respect to bare frame specimen

For the head joints, Mohr–Coulomb’s law was applied since no mortar interlocking occurred there.

The results calculated by the third approach used for the modelling of the interface elements are given in Fig. 6 and Table 11 for Specimen III/2 and for Specimens I/1–4. Fully described results obtained by use of the first and second approaches can be found in (Penava et al. 2014).

The framed-masonry failure mechanisms obtained by the numerical calculations and observed during the test are given in Fig. 7.

Energy dissipation capacity,  $E$  (kNm<sup>2</sup>), is calculated as a sum of all areas within the loops until yielding of the frame infill system was reached. A comparison between experimental and numerical results is given in Fig. 8 and Table 12.

## 4 Discussion of the results

Numerical modelling of the framed-masonry specimens has been performed using simplified micromodels. Masonry units and mortar are homogenized in separate units and connected by the interface link element. The numerical results were validated against the experimental ones for specimens, with and without openings, placed at different positions. In order to achieve a satisfactory match, an adjustment (calibration) of certain parameters has been performed.

Concerning the variety of computer programs available today (e.g. Travas et al. 2009), the decision was made based on criteria described in (Al-Chaar 2008). As compared to other computer program, selected program had the ability to model in spite of the quasi-brittle nature of the masonry units by using SBeta material model (Cervenka et al. 2012). It is intended primarily for analysis of reinforced concrete and concrete structures, whether 2D or three-dimensional (3D) and is accessible to our research group. Although none of the experimental results showed out-of-plane failure, the program demonstrated its capability of simulating its possibility of occurrence when using the 3D approach.

**Table 12** Energy dissipation capacity data from tests  $E_t$  and calculations  $E_c$ 

Spec.	$E_t$ (kNmm <sup>2</sup> )	$E_c$ (kNmm <sup>2</sup> )	$E_t/E_{t,III/1}$ (–)	$E_c/E_{t,III/1}$ (–)	$(E_t - E_c)/E_t$ (%)
I/1	3793	3488	1.50	1.38	8.0
I/2	3688	4418	1.46	1.75	–19.2
I/3	5754	6473	2.28	2.56	–19.0
I/4	3899	4794	1.54	1.90	–23.6
III/1	2525	2720	1.00	1.08	–5.1
III/2	3954	4782	1.57	1.89	–21.8

#### 4.1 Selection of input parameters

Material properties were taken in terms of their mean values for all specimens in all numerical models. Standard variance of the obtained material values is tabularly presented, although it is not reflected exactly in the real and numerical models, as described in (Oberkampff and Roy 2010). Since the number of test specimens is limited, trustworthy statistical connections cannot be attained. The results obtained by the numerical model were the most sensitive concerning the values used for the bed joint interface elements. They are also the most difficult to define due to the lack of knowledge on their physical behaviour. Masonry units, with and without holes, display very different behaviours at the mortar-masonry interface. They cannot be described by the same physical law, as this could produce significant numerical errors (Penava et al. 2014).

Fracture mechanics models typically require a large amount of input data. Many of them cannot be determined through standard normative tests and/or are complex in nature, e.g., crack spacing (Bažant and Oh 1983a). Their values were assigned as recommended by appropriate literature sources (Bažant and Oh 1983a, b; Saneinejad 1990a, b; Cervenka et al. 2012; Jäger 2012). This happens to be successful in showing that the parameters, which are not described, are not crucial for the confined masonry model.

Concerning the scale of the model i.e. 1:2.5, it is assumed that no scale effect occurs, relying on the studies given in (Beyer et al. 2012). During the scaling selection, material properties of the prototype and the scaled model are meant to be the same, with the intention to keep equal the stress in columns on the prototype and in the model. In addition, the number of bed joints was the same in the model and on the prototype. Details about the scaling can be found in (Sigmund and Penava 2014).

#### 4.2 Modelling and calibration

The following problems, which caused poor behaviour of the numerical model, were encountered and solved during modelling of the bare RC frame (Specimen III/1).

- Since reinforcement bars in the frame were modelled as truss elements, their bending and shear stiffness somehow had to be taken into account. The problem was solved by increasing the transverse reinforcement for the amount of the longitudinal.
- Tension softening was observed at the columns' bases (plastic hinges). The problem was solved by the inclusion of tension stiffening and crack spacing parameters in the RC model.

Numerical modelling of the framed-masonry specimens required a more elaborate and time-consuming approach. Since the FEM program used was incapable of representing the

orthotropic masonry units, they were modelled as homogeneous ones. Therefore, they were pushed, rather than crushed, as was observed in tests (due to a lower horizontal compressive strength). This had to be corrected by using different interface elements for head and bed joints.

Material properties obtained by the normative tests were not sufficient for the numerical modelling. The numerical results for all specimens were obtained by use of three approaches:

1. The measured material values were used as input data for the model, while the total mean error between the calculated and measured values was about 30 %.
2. The previous model required the application of material values, which were not physically sound but were suggested in the literature (Pryl and Cervenka 2013) as the ones that give good results. The total mean error was lower for the specimen without openings (Specimen III/2 had an error of 4.7 %) than for those with openings (from 13.9 % to 22.1 %). The material values that are usually suggested were good for a framed-masonry specimen without an opening.
3. In the third approach, we have included the original cohesion function for the interface element of the bed joints. This solved the problems encountered as a consequence of the orthotropic masonry units and the mortar interlocking within the units, which increased the initial cohesion to the tensile strength of the masonry units. The total mean error between the calculated and measured values was within the engineering margin of error and could be used for further analysis.

Another problem was the inability of units to break due to the smeared crack approach used in the software. The cracks that occurred in the units lowered their strength. In the interaction with the interface elements, this led to numerical instabilities. This problem was solved by use of a proper post-peak inclination parameter for the cohesion function (Sect. 3.3.2).

Numerical modelling of a specimen without an opening was simpler and less sensitive to the modelling errors than specimens with an opening. They experienced diagonal tensile failure in the masonry, which was numerically simpler to reproduce. The specimens with an eccentric door/window opening had pronounced bed joint sliding failure in the masonry pier and were very sensitive to the quality of the interface element.

Cyclic shear resistances in Fig. 6 i.e. base shear force plotted against the inter-storey drift ratio (making the response general), showed a good correlation concerning the uncertainties involved in the experiment (Table 11). In the experiment, the ultimate shear resistance for the case with centric opening (I/2) was higher than of the solid infill wall case, although this was not the case in the numerical analysis. It is assumed that the cause lays in the stochastic character of material parameters involved in the analysis and the accompanying uncertainty in their estimate. In both, the experiment and the numerical model, cyclic force control was applied so it was difficult to accurately assess the energy dissipated by the loading cycles (Fig. 8; Table 12). The problem with force-controlled approach is poor description in the post-peak regime, i.e. the force remains constant after reaching the yield point. Before reaching the yield point, high amounts of loading cycles occur and after reaching the yield point only few. However, they provide most of the energy dissipation capacity (area within the loop). Material models are still sensitive in the post-peak regime of the cyclic loading scenarios, especially when significant cracking occur. The sensitivity is more pronounced both in numerical analysis and in experiments, when discrete elements are involved and there is a high amount of uncertainty in material parameters.

The failure mechanisms (the second criterion of successful calibration) were successfully described in all cases, as can be observed in Fig. 7. The simplified micromodel was able to successfully capture the sequenced failure of the infill wall in which an opening was present.

## 5 Conclusions

Commercial non-linear FEM packages provide a wide selection of elements, constitutive relationships and solution schemes, which researchers/engineers may use as tools for the study of framed-masonry structures. Their usage requires deep theoretical and practical engineering knowledge in order for them to be employed with confidence. A good way of gaining an insight into these issues is the validation of the results by reference to experimental ones. In our research, we used one of the packages (Cervenka Consulting 2012) for the study of RC frames infilled with masonry under cyclic lateral loading.

The input parameters required for every non-linear finite element program are geometry, choice of adequate numerical material models and material properties obtained by normative tests. The obtained numerical models of framed-masonry structures, therefore, have been calibrated, with their results validated against the experimental results. The following modelling requirements and limitations were encountered.

Elaborate non-linear numerical models are extremely sensitive to the choice of parameters. Their blind usage results in unacceptable errors, even in the “simple” bare RC frame model. The numerical model used for modelling two brittle materials with a large difference in peak load (concrete and masonry) has to be calibrated using the experimental results. The blind use of standard material values is not suggested, as the results cannot be relied upon.

In the model of reinforced concrete elements, the most important parameters were the element type used to model the reinforcement and concrete softening in tension. The reinforcing bars should be able to simulate bending and shear stiffness. Additionally, the transverse reinforcement bar closest to the joint had to be moved further away from the joint edge, while its area was increased by about 100 times in order to prevent unrealistic tension softening. In the case of a high reinforcement ratio in the plastic hinge region, it was important to include the tension stiffening and the maximum crack spacing parameters for the concrete material.

Masonry infill walls need additional degrees of freedom to describe cracking. This is achieved with the interface link element, whose cohesive law has to be chosen to match the energy absorbed in the opening of cracks.

In the model of masonry infill walls, the masonry unit type used was crucial. For hollow clay masonry units, with vertical or horizontal hollows, the interface link element had to facilitate an additional cohesion hardening–softening function. This was due to the mortar interlocking, which prevented shear sliding failure until tension failure of the unit occurred; this is defined as the limit shear strength in EN 1996-1-1 (CEN 2005). The corresponding deformation was easily evaluated based on the unit shear modulus, since the hollow clay unit was brittle and exhibited linear elastic behaviour until shear failure. For solid surfaces (perpendicular to the hollows or in the case of solid clay blocks), this additional function for modelling the cohesion was not necessary. As an orthotropic material model for the masonry unit was not available, different levels of stiffness in orthogonal directions were modelled by using different values for head and bed joint



stiffness. These were evaluated based on the masonry unit's values for the elastic modulus in corresponding directions and the properties of masonry units in the vertical direction. When combined with the interlocking of the mortar and units, this led to an effect in which the units were pushed, rather than crushed, in the numerical model. This behaviour was opposite to the one observed in the experiments. This phenomenon was especially pronounced in the case of an opening in the masonry wall when combined with a bed joint sliding failure mechanism.

It has been shown that non-linear FEM software could be used for numerical evaluation of the behaviour of the framed-masonry structures, irrespective of the presence and position of the opening. Its use should be adjusted/calibrated on the basis of the experimental values in order to keep errors within the engineering within acceptable limits for the design and/or assessment of the buildings. The available simplified micromodel, present in many non-linear FEM codes, cannot be directly used if the required input data are not readily available. Besides, the presence and position of the opening influenced the response of the applied numerical models. Interface elements' shear strength proved to be the parameter that controls the response. It could be adjusted by its increase (in our work's second approach) in relation to the experimental value because of the weaknesses of the mathematical model. The presented approach, through which we achieved a successful calibration, relies on experimentally obtained material values by introducing the original cohesion hardening–softening function.

**Acknowledgments** The research presented in this article is a part of the research project FRamed-Masonry Composites for Modelling and Standardization (FRAMA), which is supported by the Croatian Science Foundation. This support is gratefully acknowledged. From the first author to his daughter Anabela for revealing him the clay block masonry and mortar joint interlocking by playing with children cubes.

## References

- Al-Chaar GK (2008) Constitutive models for nonlinear finite element analysis of masonry prisms and infill walls. Washington, DC
- Asteris PG, Antoniou ST, Sophianopoulos DS, Chrysostomou CZ (2011a) Mathematical macromodeling of infilled frames: state of the art. *J Struct Eng* 137:1508–1517. doi:10.1061/(ASCE)ST.1943-541X.0000384
- Asteris PG, Kakaletsis DJ, Chrysostomou CZ, Smyrou E (2011b) Failure modes of in-filled frames. *Electron J Struct Eng* 11:11–20
- Asteris PG, Cotsovos DM, Chrysostomou CZ et al (2013) Mathematical micromodeling of infilled frames: state of the art. *Eng Struct* 56:1905–1921
- ATC (1998) Evaluation of earthquake damaged concrete and masonry wall buildings: basic procedures manual (FEMA 306). ATC, Redwood City
- Bažant ZP, Oh BH (1983a) Spacing of cracks in reinforced concrete. *J Struct Eng* 109:2066–2085
- Bažant ZP, Oh BH (1983b) Crack band theory for fracture of concrete. *Matériaux Constr* 16:155–177. doi:10.1007/BF02486267
- Bažant ZP, Planas J (1997) Fracture and size effect in concrete and other quasibrittle materials. CRC Press
- Beyer K, Binici B, Butenweg C et al (2012) Seismic behaviour of mixed reinforced concrete—unreinforced masonry wall structures. Pavia, Italy
- CEB (1993) CEB-FIP Model Code 90. American Society of Civil Engineers
- CEN (2004a) Eurocode 8: design of structures for earthquake resistance—part 1: general rules, seismic actions and rules for buildings (EN 1998-1:2004). European Committee for Standardization, Brussels
- CEN (2004b) Eurocode 2: Design of concrete structures—part 1-1: general rules and rules for buildings (EN 1992-1-1:2004). European Committee for Standardization, Brussels
- CEN (2005) Eurocode 6: Design of masonry structures—part 1-1: general rules for reinforced and unreinforced masonry structures (EN 1996-1-1:2005). European Committee for Standardization, Brussels

- CEN (2007) Methods of test for masonry—part 3: determination of Initial Shear Strength (EN 1052-3:2002/A1). European Committee for Standardization, Brussels
- CEN (2009) Testing hardened concrete—part 3: compressive strength of test specimens (EN 12390-3:2009). European Committee for Standardization, Brussels
- Cervenka Consulting (2012) ATENA 2D engineering computer program
- Cervenka V, Jendele L, Cervenka J (2012) ATENA program documentation part 1 theory. Cervenka Consulting Ltd., Prague
- Crisafulli FJ, Carr AJ, Park R (2000) Analytical modelling of infilled frame structures—a general review. *Bull N Z Soc Earthq Eng* 33:30–47
- Dawe JL, Liu Y, Seah CK (2001) A parametric study of masonry infilled steel frames. *Can J Civ Eng* 28:149–157. doi:10.1139/100-084
- Ellul F, D'Ayala D (2012) Realistic FE models to enable push-over non linear analysis of masonry infilled frames. *Open Constr Build Technol J* 6:213–235
- Ghosh AK, Amde AM (2002) Finite element analysis of infilled frames. *J Struct Eng* 128:881–889
- Grünthal G, Musson RMW, Schwarz J, Stucchi M (1998) European macroseismic scale 1998. Luxembourg
- Hashemi A, Mosalam KM (2006) Shake-table experiment on reinforced concrete structure containing masonry infill wall. *Earthq Eng Struct Dyn* 35:1827–1852
- Hillerborg A, Modéer M, Petersson PE (1976) Analysis of crack formation and crack growth in concrete by means of fracture mechanics and finite elements. *Cem Concr Res* 6:773–781
- Jäger W (2012) Mauerwerk-Kalender 2012: Schwerpunkt: Eurocode 6. Ernst & Sohn
- Lourenço PB, Rots JG, Blaauwendraad J (1995) Two approaches for the analysis of masonry structures: micro and macro modelling. *Heron* 40:313–340
- Meharbi AB, Shing BP (2003) Seismic analysis of masonry-infilled reinforced concrete frames. *TMS J* 21:81–94
- Negro P, Colombo A (1997) Irregularities induced by nonstructural masonry panels in framed buildings. *Eng Struct* 19:576–585
- Neufert E, Neufert P (2012) Architects' data, 4th edn. Wiley-Blackwell, New York
- Oberkampf WL, Roy CJ (2010) Verification and validation in scientific computation. Cambridge University Press, Cambridge
- Penava D (2012) Influence of openings on seismic response of masonry infilled reinforced concrete frames. Josip Juraj Strossmayer University of Osijek, Osijek
- Penava D, Sigmund V, Kožar I (2014) Micro modeling of tested framed-wall with openings. In: Proceedings of the 2nd European conference on earthquake engineering and seismology. Istanbul, Turkey, pp 279–289
- Pryl D, Cervenka J (2013) ATENA program documentation, part 1 of 1, troubleshooting manual. Cervenka Consulting Ltd., Prague
- Saneinejad A (1990a) Non-linear analysis of infilled frames Part 2. University of Sheffield, Sheffield
- Saneinejad A (1990b) Non-linear analysis of infilled frames Part 1. University of Sheffield, Sheffield
- Sigmund V, Penava D (2014) Influence of openings, with and without confinement, on cyclic response of infilled r-c frames—an experimental study. *J Earthq Eng* 18:113–146
- Tomažević M (1999) Earthquake-resistant design of masonry buildings. Imperial College Press, London
- Travas V, Ozbolt J, Kozar I (2009) Failure of plain concrete beam at impact load: 3D finite element analysis. *Int J Fract* 160:31–41